J Nanostruct 16(1): 1017-1033, Winter 2026

RESEARCH PAPER

Laser Energy and SnO_2-Doping Effects on Structural, Morphological, and Optical Properties of GeO_2 Thin Films Prepared by PLD

Mohammed Nife Gaser [1], *Hossain Milani Moghaddam* [1], *Mahdi Mohmoud Mutter* [2*]

[1] *Department of Solid-State Physics, Faculty of Basic Sciences, University of Mazandaran, 4741695447, Babolsar, Iran*

[2] *Scientific Research Commission, Baghdad, Iraq*

ARTICLE INFO

Article History:
Received 27 September 2025
Accepted 18 December 2025
Published 01 January 2026

Keywords:
Energy gap
GeO2 Thin Films
Nanoparticle Refinement
PLD
SnO_2 Doping

ABSTRACT

This study successfully investigated the structural, morphological, and optical tunability of Germanium Dioxide (GeO_2) thin films for potential optoelectronic applications. The films were prepared on Silicon (Si) substrates at ambient temperature using the Pulsed Laser Deposition (PLD) technique, systematically varying the laser energy (200 mJ to 350 mJ) and the SnO_2 doping concentration (1 wt% to 908 wt%). High laser energy resulted in a consistent decrease in both AFM grain size (90.01 nm to 65.01 nm) and SEM particle size (58.68 nm to 22.24 nm), while simultaneously causing an increase in RMS roughness (15.6 nm to 25.1 nm) and widening the direct band gap (E_g) (3.55 eV to 3.65 eV). Conversely, SnO_2 doping dramatically modifies the surface morphology, causing a consistent increase in AFM grain size and RMS roughness (up to 105.34 nm and 60.4 nm respectively), while the SEM particle size exhibited a non-monotonic trend, achieving the minimum size (18.73 nm) at 5 wt%. Optically, the SnO_2 dopant caused a complex shift in E_g, with an initial widening to a maximum of 3.65 eV at 2 wt% followed by E_g narrowing to a minimum of 3.40 eV at 5 wt%. UV absorption consistently peaked at 290 nm and its magnitude generally increased with both higher laser energy and higher doping. The PLD method provides effective dual control: high laser energy enhances structural quality and E_g widening, while SnO_2 doping offers fine-tuning, particularly by introducing electronic effects that cause band gap narrowing at higher concentrations.

How to cite this article
Nife Gaser M., Milani Moghaddam H., Mohmoud Mutter M. Laser Energy and SnO_2-Doping Effects on Structural, Morphological, and Optical Properties of GeO_2 Thin Films Prepared by PLD. J Nanostruct, 2026; 16(1):1017-1033. DOI: 10.22052/JNS.2026.01.091

INTRODUCTION

Semiconductors are the cornerstone of modern electronic and optoelectronic technology, facilitating devices from integrated circuits to sensors [1]. Precise control over their electronic band structure is crucial. Among these, metal-oxide semiconductors (MOS) like ZnO, SnO_2, and GeO_2 are highly valued for their stability, wide bandgap (WBG) characteristics, and cost-effectiveness [2]. Their versatility makes them indispensable for next-generation transparent

* *Corresponding Author Email: mahdimutter@yahoo.com*

electronics, UV detectors, and chemical gas sensors. Recent advancements emphasize the crucial role of controlling material dimensions at the nanoscale, where structural evolution significantly impacts electronic performance, necessitating continuous research into advanced synthesis methods [3]. Germanium dioxide (GeO_2) is a particularly interesting WBG metal oxide. Crystalline GeO_2 exhibits a direct bandgap typically in the range of 4.5-5.5 eV, making it highly promising for deep UV applications and as a high-k dielectric material in microelectronics due to its high breakdown field strength and compatibility with Germanium substrates [4]. GeO_2 is also a key material for integrated photonics due to its role as a host for luminescence and optical amplification [5]. However, tailoring GeO_2 films often requires introducing defects or impurities to narrow the bandgap or enhance conductivity, especially for sensing applications where surface conductance changes are key. The structural crystallinity, surface morphology, and optical absorption edge of GeO_2 thin films are highly sensitive to deposition parameters, making the choice of synthesis technique and subsequent post-processing steps critical. Achieving high-quality thin films requires precise control over stoichiometry and crystallinity. Pulsed Laser Deposition (PLD) is a superior technique for synthesizing complex oxide thin films due to its ability to maintain target stoichiometry, high deposition rate, and versatility [6]. Laser energy is a critical operational parameter in PLD, directly influencing the kinetic energy of ablated species, plasma temperature, and consequently, the film's crystallinity, grain size, and defect concentration [7]. PLD enables non-equilibrium growth conditions, ideal for synthesizing metastable phases or inducing beneficial stress/strain, thereby enhancing functional properties [8]. Manipulating the laser energy offers a non-chemical pathway to control the structural and morphological features, which fundamentally dictate the optical and electronic properties of the resulting thin film. Therefore, a systematic study on the effect of varying laser energy is essential to optimize the growth parameters of GeO_2 and GeO_2: SnO_2 thin films. To enhance GeO_2 functional performance, particularly for gas sensing and optical properties, Tin Oxide (SnO_2) is introduced as a dopant. SnO_2 is a well-known n-type MOS with a wide bandgap (sim 3.6 eV) and excellent chemical sensitivity [9]. Integrating SnO_2 into the GeO_2 matrix is expected to create synergistic effects, leading to structural modifications and localized electronic states within the GeO_2 bandgap. Introducing Sn ions can cause changes in lattice constant, crystal structure distortion, and the formation of oxygen vacancies, which are critical for surface chemical reactions and carrier mobility [10]. Substitutional doping mechanisms often lead to non-linear property changes due to competing effects of lattice strain and charge carrier concentration [11]. Furthermore, the interplay between the host (GeO_2) and the dopant (SnO_2) can be exploited for band gap engineering, allowing precise tuning of the film's absorption edge for optoelectronic devices. Controlling the doping concentration is paramount, as an optimal amount can dramatically improve performance, while excessive doping often leads to phase segregation or crystallinity degradation. This study is therefore primarily focused on systematically investigating the dual influence of pulsed laser deposition energy (200-350 mJ) and SnO_2 doping concentration (1, 2, 3, 5, 8 wt%) on the fundamental physical properties of GeO_2 thin films deposited at room temperature. The primary objectives are: (1) To determine the effect of varying laser energy on the crystallinity, preferred orientation, and grain size of both pure and Sn-doped GeO_2 films using XRD. (2) To analyze the evolution of surface morphology, grain distribution, and roughness via AFM and SEM. (3) To precisely calculate and correlate the optical constants, specifically (α) and the direct optical bandgap (Eg), with the induced structural and morphological changes by utilizing UV-Visible Spectroscopy. The insights gained will contribute significantly to the optimization of GeO_2: SnO_2 based materials for transparent electronic and sensor applications, providing valuable data for controlled synthesis via PLD.

MATERIALS AND METHODS

Target Materials

The base material used was high-purity Germanium Dioxide (GeO_2) powder (99.999% purity, Sigma-Aldrich). The dopant material was high-purity Tin Oxide (SnO_2) powder (99.99% purity, Sigma-Aldrich).

Target preparation

The GeO_2:SnO_2 targets were prepared for PLD by the standard solid-state reaction and cold

pressing method. SnO_2 powder was mixed with GeO_2 powder at varying concentrations: 1, 2, 3, 5, and 8 weight percent (wt%) of SnO_2. The pure GeO_2 powder target was also prepared for comparison. The powders were thoroughly mixed and ground in an agate mortar for approximately 30 minutes to ensure homogeneity. The mixed powders were pressed into circular pellets (20 mm diameter) under a pressure of 5-10 tons for 10 minutes using a hydraulic press. The resulting pellets were subjected to a high-temperature sintering process in an ambient air atmosphere at a temperature of 800-900 °C for 6 hours to increase their density and mechanical stability, crucial for effective laser ablation.

PLD System Setup

The thin films were deposited using an in-house customized PLD system (e.g., using a high vacuum chamber).

Laser Source

- Laser Type: Nd: YAG pulsed laser (e.g., Continuum Surelite III) operating at its fourth harmonic (λ= 266 nm) to ensure strong absorption by the oxide targets.
- Pulse Duration: Typically, 5-10 ns.
- Repetition Rate: Set to 5 Hz (pulses per second).
- Pulse Number: A fixed number of 100 laser pulses was applied for the deposition of each film to control the film thickness.
- Laser Energy Variation: The impact of laser energy was investigated by varying the laser energy density hitting the target at: 200, 250, 300, and 350 mJ.

Deposition Parameters

All films were deposited at room temperature on Si substrate to investigate low-temperature film growth. The deposition chamber was evacuated to a high vacuum pressure of 10^{-5} Torr. Maintained constant at 5 cm. The target was rotated during deposition to ensure uniform ablation and prevent pitting. The obtained samples thermal treatment a 750 °C for annealing. The thickness of the prepared thin films was measured using an ellipsometer technique (Gaertner L116C). Since the number of pulses (100) was fixed, Table 1 presents the thickness measurements of samples produced at room temperature with varying laser energy between 200 and 350 mJ, using a constant number of 100 pulses on the glass substrates (it is noteworthy that the thickness measurements exhibited an error margin of around 5.2 nm). While the laser energy rises, the overall thickness of these films also increases, indicating that higher laser energy results in the removal of more particles from the target area. Consequently, the thickness of these thin films escalates.

Characterization Techniques

The structural, morphological, elemental, and optical properties of the GeO_2 and GeO_2:SnO_2 thin films were investigated using the following high-precision instruments: X-ray Diffraction (XRD) was using type (Bruker D8 Advance system). Atomic Force Microscopy (AFM)was using type (AFM Veeco Dimension 3100). Scanning Electron Microscopy was using type (SEM) (SEMFEI Quanta FEG). UV-Visible Spectroscopy was using type (Shimadzu UV-1800spectrophotometer).

RESULTS AND DISCISSION

Fig. 1 and Table 2, derived from the X-ray Diffraction (XRD) patterns, confirms the structural evolution of the pure GeO_2 thin films as a function of the Pulsed Laser Deposition (PLD) laser energy (200, 250, 300, and 350 mJ). The crystallite size (D) is the critical parameter quantified from the XRD data. It is calculated using the Scherrer equation of the diffraction peaks (Scherrer, 1918) [12]:

Table 1. Thickness of GeO_2:SnO_2 thin film.

Samples	Thickness nm(±5.2 nm).			
	Laser energy mJ			
	200 mJ	250 mJ	300 mJ	350 mJ
GeO_2	201	224	241	255
GeO_2:1wt%SnO_2	201	224	243	259
GeO_2:2wt%SnO_2	201	224	244	260
GeO_2:3wt%SnO_2	201	224	246	260
GeO_2:5wt%SnO_2	201	224	248	261
GeO_2:8wt%SnO_2	201	224	247	263

$$D = \frac{K\lambda}{\beta\cos\theta} \quad (1)$$

Where D is the crystallite size, K is the shape factor (typically 0.94), λ is the X-ray wavelength (CuKα), β is the FWHM (in radians), and θ is the Bragg angle.

The films are confirmed to be polycrystalline and possess the hexagonal crystal structure of GeO_2 across all deposited energies, consistent with the standard reference card (Card No. 98−020−0731). Five main diffraction planes are observed: (010), (011), (110), (102), and (020). The presence of multiple peaks confirms the polycrystalline nature. The Experimental d-spacing (D-space. Exper.) values are in excellent agreement with the Standard d-spacing (d-space. Stand.) values for all peaks and laser energies. This highly consistent match validates the phase purity, confirming the material is indeed hexagonal GeO_2 with minimal lattice distortion or secondary phases. Fig. 2 shows a clear dependence of the average crystallite size on laser energy. The data exhibits a monotonic increase in the average crystallite size from 24.938 nm at 200 mJ to 29.228 nm at 350 mJ. This positive correlation suggests that higher laser energy in this range provides greater kinetic energy to the ablated plasma plume species. This energy translates into increased surface adatom

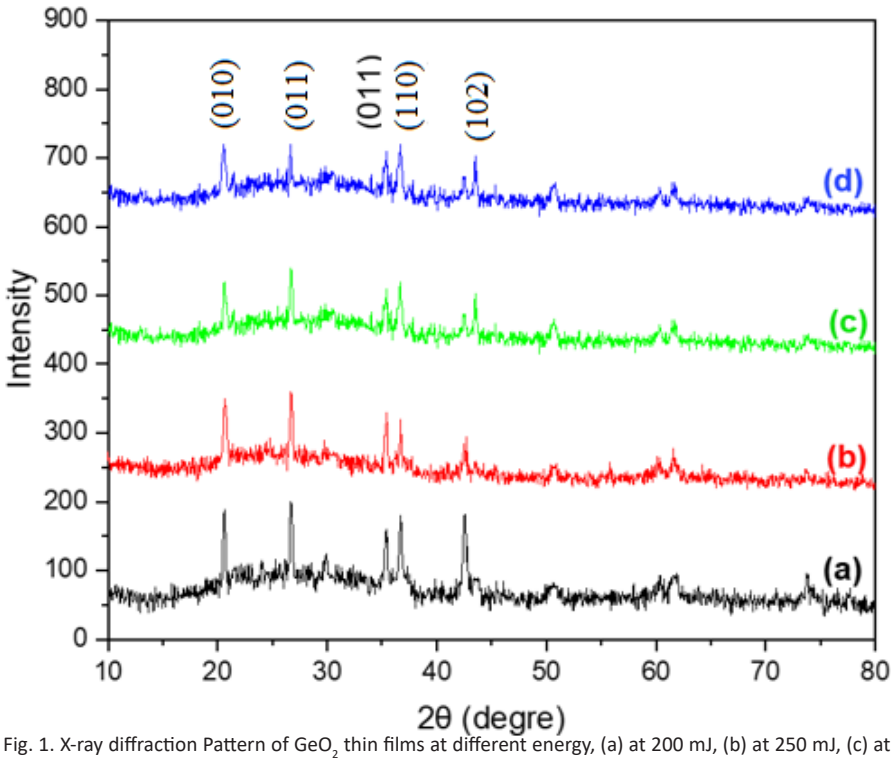

Fig. 1. X-ray diffraction Pattern of GeO_2 thin films at different energy, (a) at 200 mJ, (b) at 250 mJ, (c) at 300 mJ, (d) at 350 mJ.

Table 2. Crystal structure of GeO_2 on a silicon base at various pulses (200,250,300, and 350).

Laser Energy (mJ)	2θ (011) (degree)	FWHM (011) (rad)	Crystallite Size (011) (nm)	Average Crystallite Size (nm)
200	26.714	0.670	13.360	24.938
250	26.725	0.328	27.220	26.914
300	26.830	0.528	17.240	28.778
350	26.910	0.357	25.910	29.228

mobility upon condensation on the substrate, promoting the formation of larger, better-defined crystalline domains, thus enhancing the overall crystallinity of the film [13]. While some PLD studies on metal oxides (e.g., ZnO or TiO_2) show that excessively high laser energies can cause plasma overheating and rapid nucleation, leading to smaller crystallites, the results here for GeO_2 show the opposite trend (increasing size). This implies that the energy threshold for achieving maximum crystal growth in GeO_2 films via PLD is at or above 350 mJ under these specific deposition conditions (room temperature, silicon substrate). Research by Kumar et al. (2023) [14], on oxide films supports the idea that optimizing PLD parameters is crucial. In systems where the film

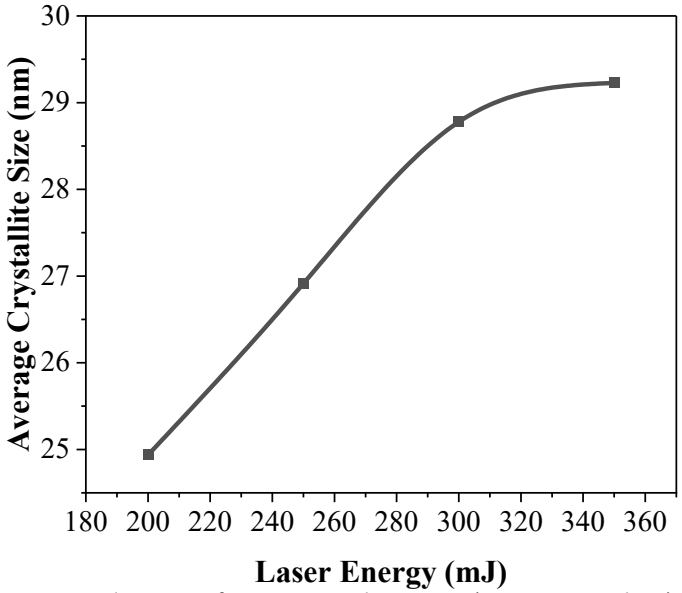

Fig. 2. Crystal structure of GeO_2 at various laser energy (200,250,300, and 350).

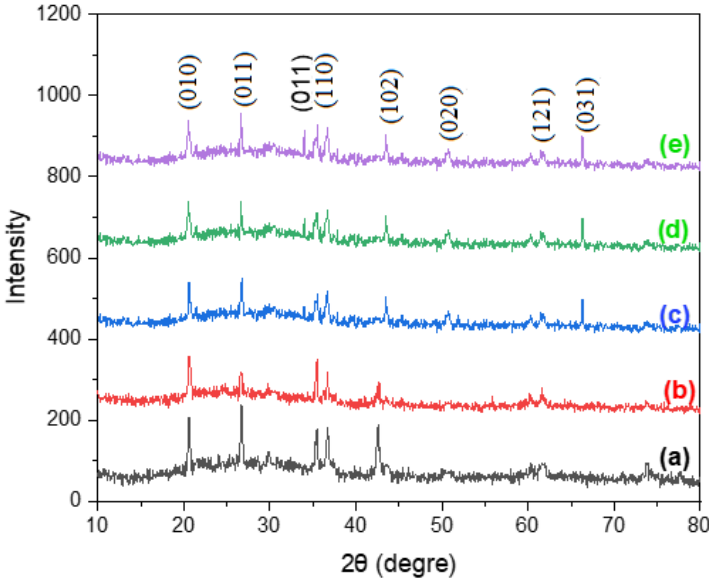

Fig. 3. XRD of GeO_2:SnO_2 thin films, (a) GeO_2:1wt%SnO_2, (b) GeO_2:2wt%SnO_2, (c) GeO_2:3wt%SnO_2, (d) GeO_2:5wt%SnO_2, and (e)GeO_2:8wt%SnO_2.

is under structural constraint (such as GeO_2 on Si), increasing the kinetic energy (via higher laser energy) can sometimes provide the necessary activation energy to overcome potential barriers for grain boundary movement, thus promoting crystal growth. These results establish the baseline for the undoped films. The subsequent analysis of the SnO_2-doped films must consider this established trend, as the introduction of SnO_2 is likely to introduce strain and defects, competing with the growth-promoting effect of the laser energy [15].

Fig. 3 and Table 3 detail the effect of SnO_2 doping concentration (from 1 wt% to 8 wt%) on the structural parameters of the GeO_2 thin films prepared by PLD at laser energy 350 mJ. The GeO_2 films primarily retain the hexagonal structure (Card No. 98−020−0731), but the appearance of new peaks, such as (121) and (031), indexed to the Tetragonal phase (Card No. 98−001−6635), is noted, particularly at higher concentrations (5 wt% and 8 wt%).This confirms that doping with SnO_2 (which itself is typically tetragonal rutile structure) induces a mixed-phase regime or high lattice strain in the host GeO_2 matrix [15].The hexagonal (011) peak remains a dominant orientation across all samples, but its intensity and FWHM fluctuate with SnO_2 ratio. A slight shift in the 2θ values for the main peaks (2θ for (011) shifts from 26.714◦ at 1 wt% to 26.93◦ at 8 wt%) indicates a

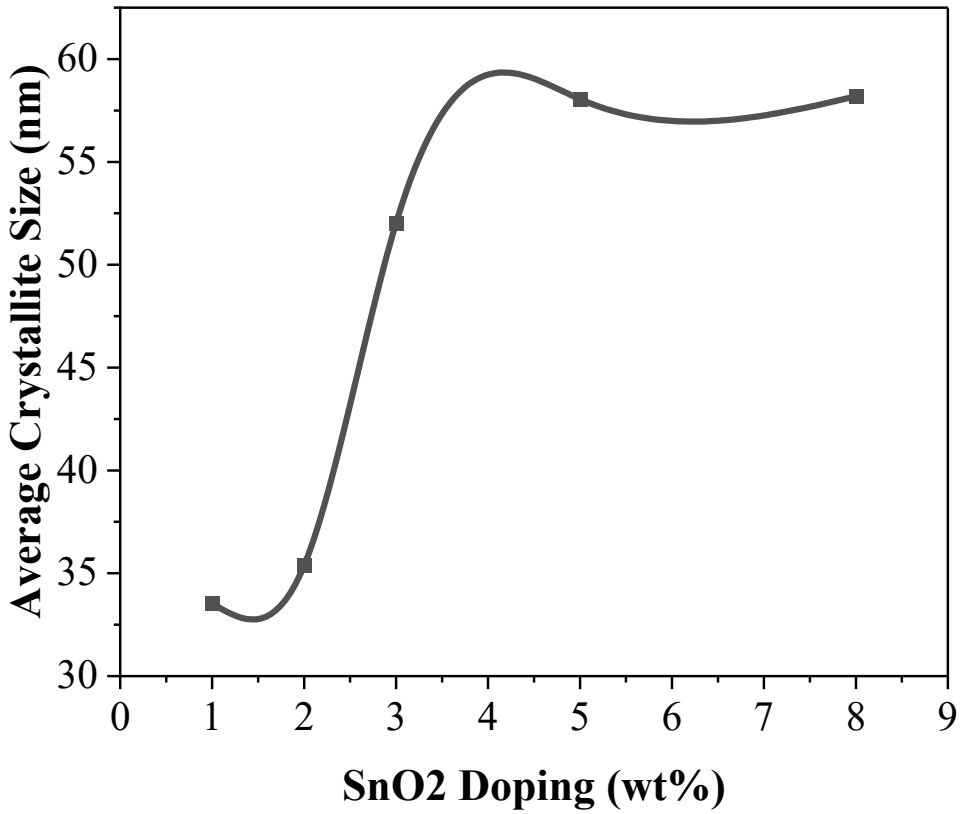

Fig. 4. The SnO_2 doping via average crystallin size of GeO_2:SnO_2 thin films.

Table 3. showing the essential parameters for the main (011) hexagonal peak and the overall structural conclusion.

Sample Name (wt%SnO2)	2θ (011) (degree)	FWHM (011) (rad)	Crystallite Size (011) (nm)	Average Crystallite Size (nm)
1 wt%	26.814	0.680	13.180	33.53
2 wt%	26.733	0.422	21.220	35.39
3 wt%	26.740	0.528	17.220	52.035
5 wt%	26.900	0.467	19.200	58.05
8 wt%	26.930	0.321	27.950	58.19

change in the d-spacing. This suggests that the Sn atoms (which have a different ionic radius than Ge) are being incorporated, leading to lattice distortion/strain within the GeO_2 host structure, as predicted by the standard Vegard's law effects [14]. The Average Crystallite Size shows a strong dependence on the SnO_2 doping concentration, as shown in Fig. 4. The average crystallite size initially increases significantly with SnO_2 doping, rising sharply from 35.39 nm (2 wt%) to 52.035 nm (3 wt%). The size continues to increase up to 58.05 nm (5 wt%) but then saturates at 58.19 nm (8 wt%). The addition of SnO_2 acts as a crystal growth enhancer up to an optimum concentration (~5 wt%). This enhancement is likely due to the Sn dopant providing energy during the deposition process that aids the GeO_2 grain boundary movement, leading to larger grains. However, at

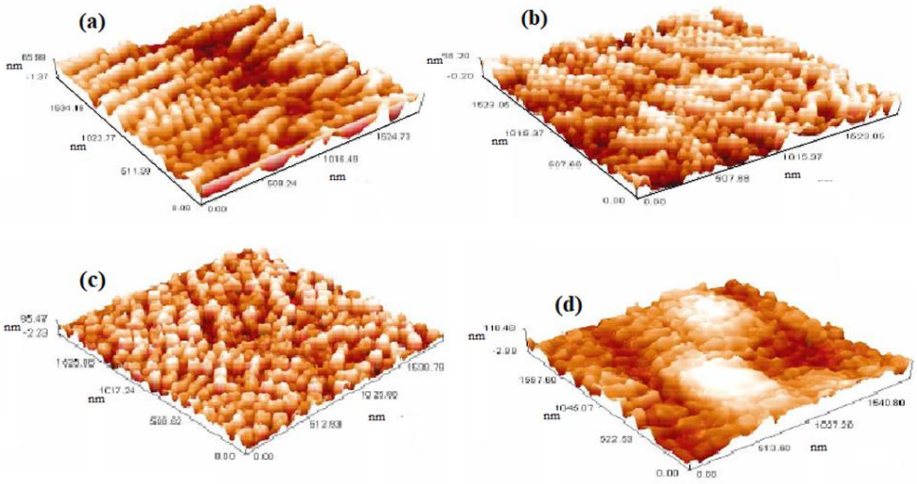

Fig. 5. AFM images of GeO2 thin films, (a) at 200 mJ, (b) at 250 mJ, (c) at 300 mJ, (d) at 350 mJ.

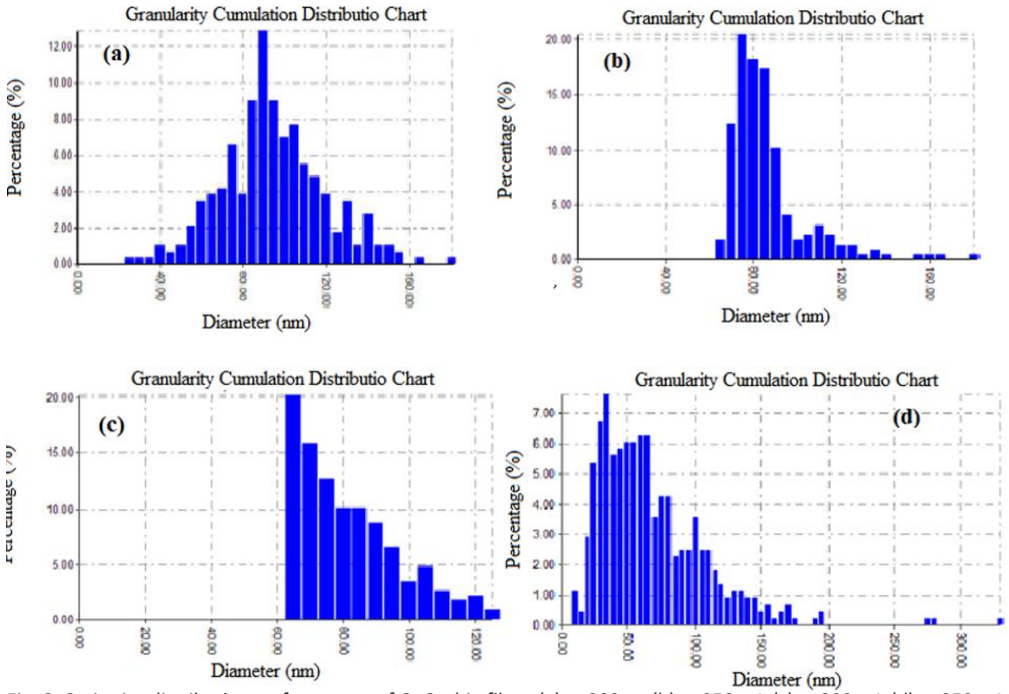

Fig. 6. Grain size distribution surface count of GeO_2 thin films, (a) at 200 m, (b) at 250 mJ, (c) at 300 mJ, (d) at 350 mJ.

very high concentrations (8 wt%), the beneficial effect saturates, possibly because the increasing lattice strain counteracts further growth.

Atomic Force Microscopy (AFM) was used to investigate the surface topography, grain size, and roughness characteristics of undoped GeO_2 thin films deposited via PLD. The AFM micrographs confirm high film uniformity and excellent adhesion. The morphological parameters, summarized in Table 4, show that the average grain size is consistently below 100 nm.A significant morphological transition was observed as the incident laser energy increased from 200 mJ to 350 mJ. This increase resulted in a systematic reduction

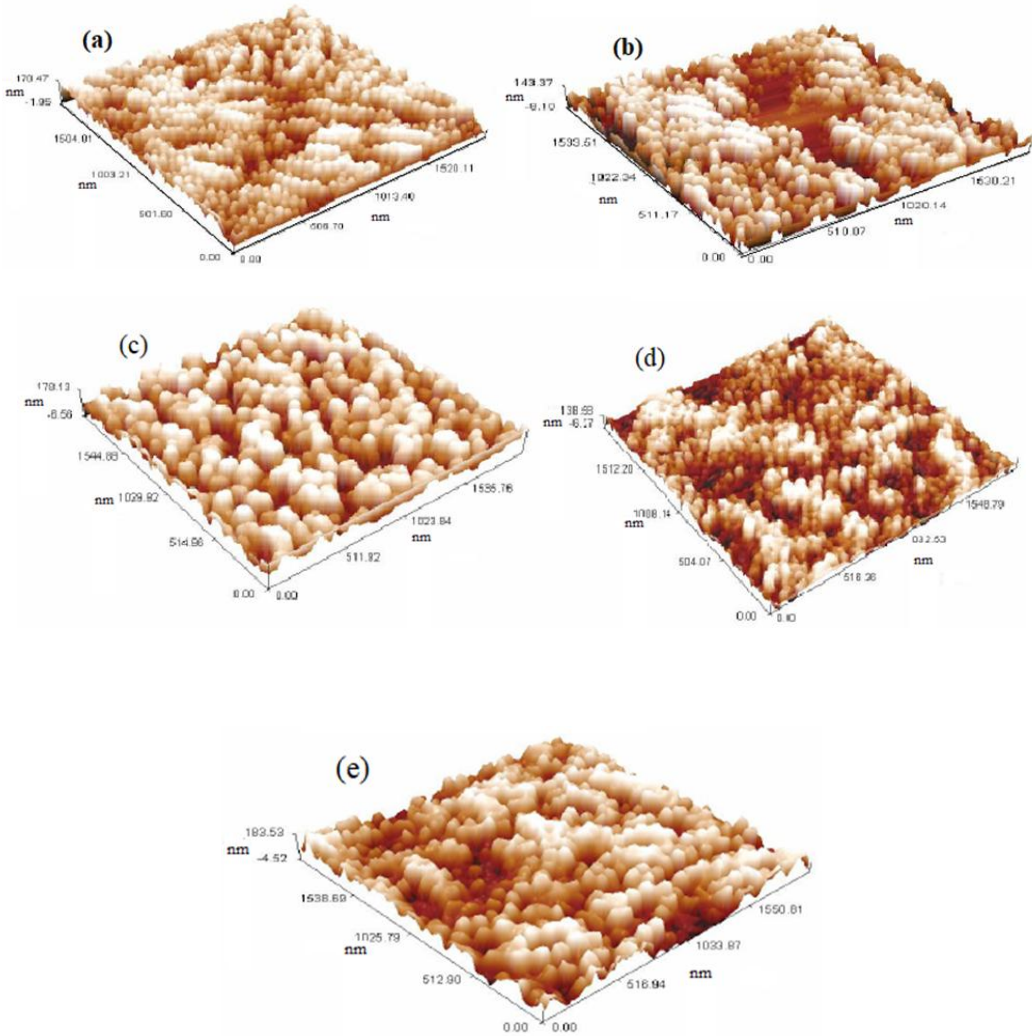

Fig. 7. AFM images of GeO_2:SnO_2 thin films at 350 mJ, (a) GeO_2:1wt%SnO_2, (b) GeO_2:2wt%SnO_2, (c) GeO_2:3wt%SnO_2, (d) GeO_2:5wt%SnO_2, (e) GeO_2:8wt%SnO_2.

Table 4. AFM data for GeO_2 thin films at various laser energy.

Samples	Laser energy (mJ)	Grain size (nm)	Roughness (nm)	Root Mean Square (nm)
GeO_2	200	90.01	13.1	15.6
	250	81.66	15.1	17.8
	300	78.10	18.8	21.2
	350	65.01	20.2	25.1

in average grain size (decreasing from 90.01 nm to 65.01 nm). Conversely, both the average roughness (Ra) and the RMS roughness showed a marked increase (escalating from 13.1 nm and 15.6 nm to 20.2 nm and 25.1 nm, respectively). This dual trend (decreasing grain size and increasing roughness) is rooted in the dynamics of the PLD plume [16]. Increasing laser energy boosts the kinetic energy and flux of ablated species [17], resulting in the ejection of smaller particles that strike the substrate with higher energy. This high arrival rate and low surface mobility promote a significantly higher nucleation rate and hinder particle coalescence. Consequently, the film develops a denser structure of smaller crystallites, contributing to the measured increase in surface irregularities [18]. The particle distribution analysis (Fig. 6) further supports this conclusion, showing

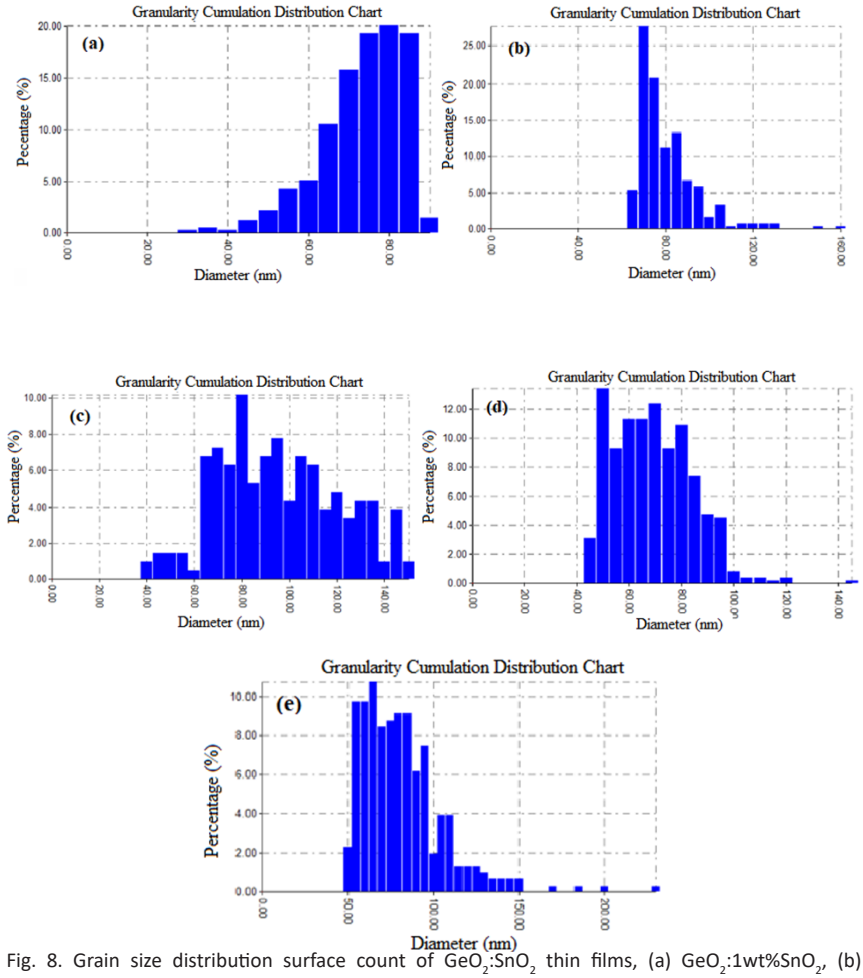

Fig. 8. Grain size distribution surface count of GeO_2:SnO_2 thin films, (a) GeO_2:1wt%SnO_2, (b) GeO_2:2wt%SnO_2, (c) GeO_2:3wt%SnO_2, (d) GeO_2:5wt%SnO_2, (e) GeO_2:8wt%SnO_2.

Table 5. AFM data for GeO_2:SnO_2 thin films at 350 mJ.

Samples	Grain size (nm)	Roughness (nm)	Root Mean Square (nm)
GeO_2:1wt%SnO_2	71.06	33.3	34.5
GeO_2:2wt%SnO_2	78.40	38.1	45.7
GeO_2:3wt%SnO_2	92.15	43.5	50.2
GeO_2:5wt%SnO_2	97.07	50.1	56.3
GeO_2:8wt%SnO_2	105.34	56.7	60.4

a clear shift towards smaller, more dominant size classes at higher deposition energy. This observed dependence is consistent with findings for other PLD oxide thin films, confirming that elevated kinetic energy of the plasma plume is a dominant factor in controlling grain refinement and surface morphology [18].

The surface morphology of GeO_2 thin films doped with SnO_2 (1 wt% to 8 wt%) was studied using AFM at an optimized laser energy of 350 mJ. Unlike the inverse relationship observed when increasing laser energy, increasing the SnO_2 concentration leads to a simultaneous increase in both the average grain size and the surface roughness parameters (Table 5). Specifically, the average grain size systematically increases from 71.06 nm to105.34 nm. Concurrently, the RMS roughness dramatically escalates from 34.5 nm to a maximum of 60.4 nm for the 8 wt% film. The observed increase in grain size and roughness is attributed to the Sn dopant modifying film growth kinetics [18]. The incorporation of Sn atoms promotes two primary mechanisms: enhanced surface diffusion, which lowers the kinetic

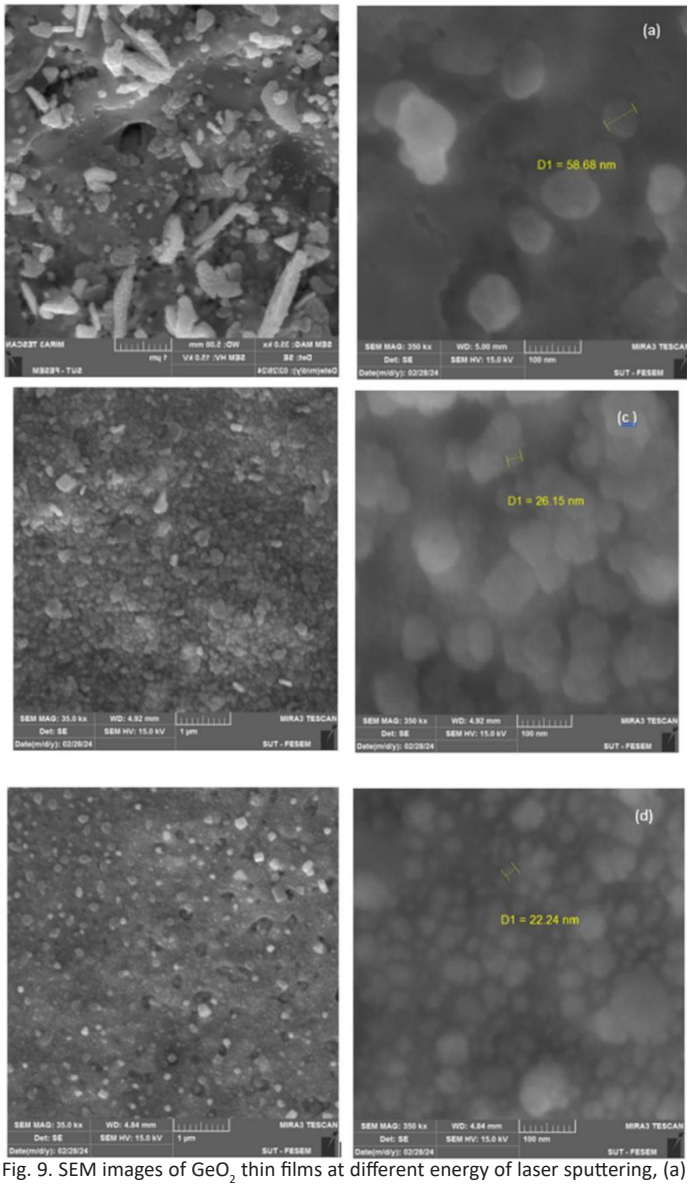

Fig. 9. SEM images of GeO_2 thin films at different energy of laser sputtering, (a) at 200 mJ, (b) at 250 mJ, (c) at 300 mJ, (d) at 350 mJ.

barrier enabling adatoms to coalesce into larger structures [19], and strain-induced nucleation, where doping-induced strain or the formation of secondary SnO_2 phases favors the growth of fewer, larger grains [20]. This change confirms that SnO_2 acts as a structural modifier, shifting the growth mode toward a more three-dimensional island-like growth as the concentration rises.

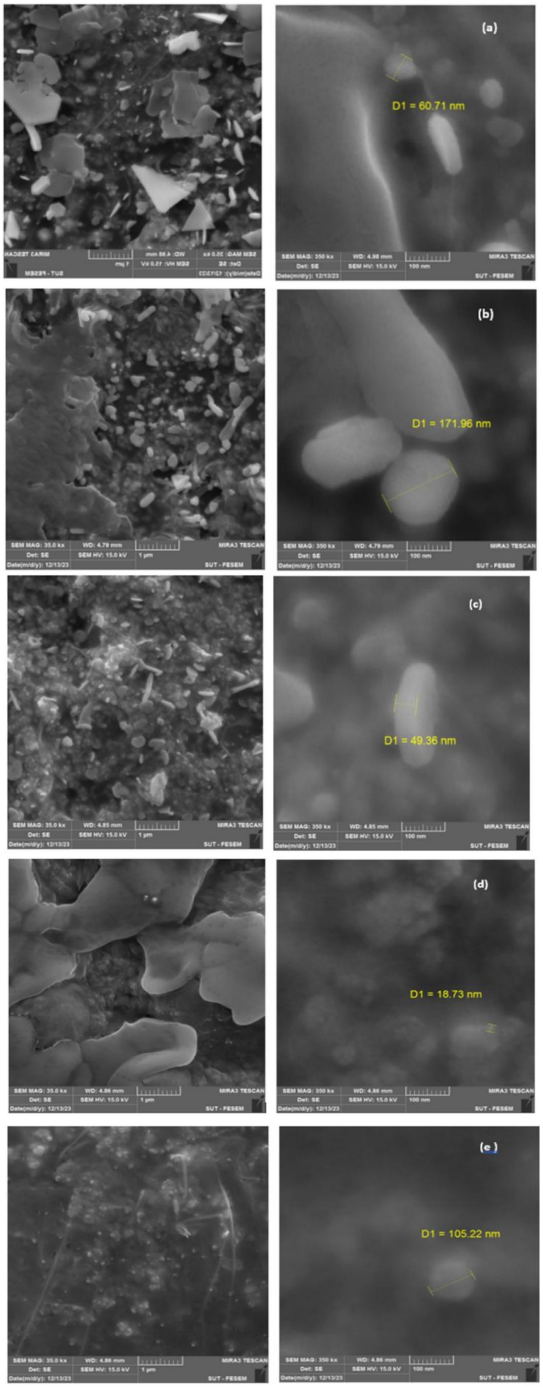

Fig. 10. SEM images of GeO_2:SnO_2, (a) GeO_2:1wt%SnO_2, (b) GeO_2:2wt%SnO_2, (c) GeO_2:3wt%SnO_2, (d) GeO_2:5wt%SnO_2, (e) GeO_2:8wt%SnO_2.

The surface morphology of the pure GeO_2 thin films prepared via Pulsed Laser Deposition (PLD) was further investigated using Scanning Electron Microscopy (SEM). The SEM micrographs, presented in Fig. 9, confirm that the synthesized films consist of nanoparticles generally measuring less than 100 nm. The particle shapes are predominantly spherical, although some irregular and aggregated clusters are observable across all samples. This nanoscale morphology confirms the suitability of the PLD technique for producing high-performance GeO_2 thin films. The images, captured at varying magnifications (micron and 100 nm scales), show that the films exhibit uniform homogeneity with minimal aggregation, attesting to the quality of the deposited coating. A critical observation derived from the precise size measurements (extracted using ImageJ software) is the dependency of the particle size on the incident laser energy, where the results showed that the particle size systematically decreased from 58.68 nm at 200 mJ to a minimum of 22.24 nm at 350 mJ. This trend nanoparticle size reduction with increased laser energy is attributed to the fundamental PLD mechanism. Higher laser energy enhances the momentum transfer to the target material, resulting in a plasma plume composed of species with higher kinetic energy and increased ablation speed [21]. This rapid ejection minimizes the time available for ablated particles to collide and aggregate within the plume before reaching the substrate, thereby reducing the size of the deposited nanoparticles [22]. These findings are strongly corroborated by recent literature concerning PLD growth of oxide nanomaterials. The observed inverse relationship between laser energy and particle size is consistent with the results reported by [23], who studied similar oxide nanostructures. Furthermore, this confirms the general understanding that increasing laser energy is an effective strategy for achieving finer nanoscale features in oxide thin films deposited by PLD [22].

The morphology of GeO_2 thin films doped with SnO_2 (1wt% to 8 wt%) was investigated using SEM at a fixed laser energy of 350 mJ. SEM micrographs (Fig. 10) revealed a consistent surface pattern of homogeneous porous structures composed of

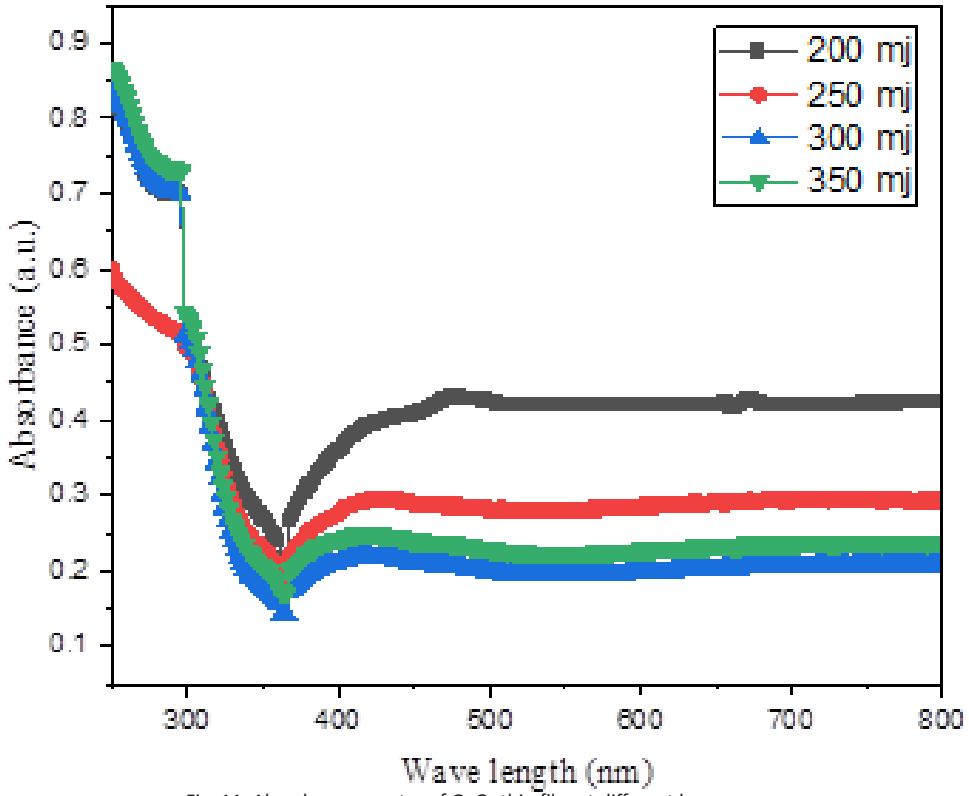

Fig. 11. Absorbance spectra of GeO_2 thin film at different laser power.

semi-spherical nanoparticles. The average particle diameter showed a complex, non-monotonic dependence on SnO_2 concentration (Table 6). Ignoring anomalies at 2 wt% (171.96 nm) and 8 wt% (105.22 nm) attributed to technical system issues, the dominant trend showed nanoparticle size reduction with increasing doping, reaching a minimum of 18.73 nm at 5 wt%. This contrasts with the systematic increase in AFM grain size and roughness. The mechanism for this SEM particle size reduction (or intra-plume refinement) at specific doping levels is ascribed to the interaction between the pulsed laser and the larger ionic radius of Sn^{+4} relative to Ge^{+4} [24, 25]. This interaction potentially leads to Dopant Disruption of larger GeO_2 clusters in the plume and Surface Strain upon deposition, favoring smaller, stable nanoparticles. While AFM showed inter-grain coalescence (macro-scale roughening), SEM indicates this concurrent nano-scale refinement, underscoring the precise morphological control achievable via PLD [26].

The optical absorption properties of the pure GeO_2 thin films deposited on Si substrates using PLD at varying laser energies (200 to 350 mJ) were investigated by measuring the absorption spectrum in the wavelength range of 230 nm to 800 nm. As illustrated in Fig. 11, all prepared films exhibit high fundamental absorption within the ultraviolet (UV) region, specifically at wavelengths between 230 nm and 300 nm. This strong absorption peak is characteristic of semiconductor materials and is attributed to interbond electronic transitions, where valence band electrons are excited across the energy gap to the conduction band upon absorbing high-energy UV photons. Beyond 350 nm (into the visible spectrum), the absorption rapidly decreases due to the

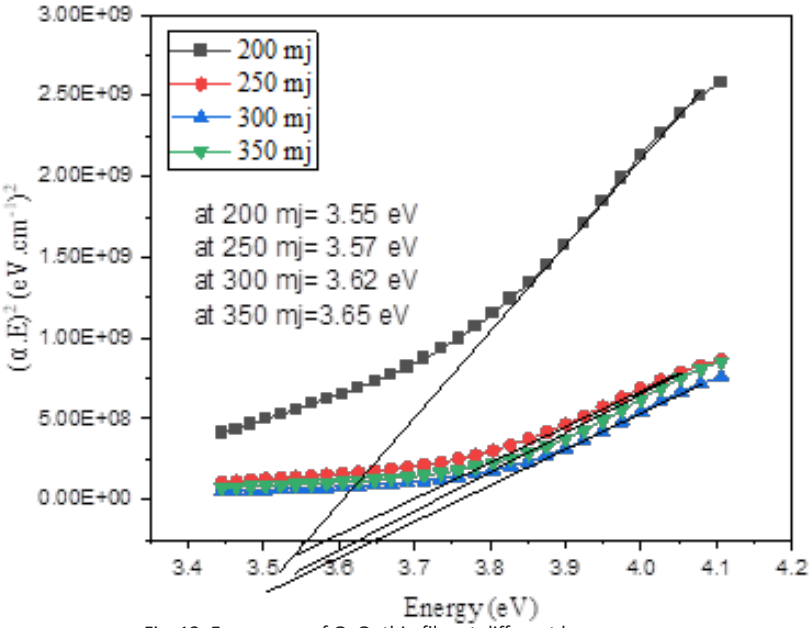

Fig. 12. Energy gap of GeO_2 thin film at different laser power.

Table 6. The E_g of GeO_2 for different laser energy.

Laser Energy (mJ)	Direct Band Gap (Eg) (eV)
200	3.55
250	3.57
300	3.62
350	3.65

weak photon energy corresponding to longer wavelengths. A slight but systematic variation in absorbance values is observed based on the laser energy used for deposition, where, the film prepared at 350 mJ exhibits the highest absorbance (0.97), followed sequentially by films prepared at 300 mJ, 250 mJ, and 200 mJ. Also, the maximum difference in absorbance between the highest (350 mJ) and lowest energy films is minimal (0.02). This enhancement in absorbance with increasing laser energy is primarily correlated with the resulting film morphology and thickness. The higher absorbance is plausibly ascribed to the increased film thickness (typical at higher laser energy), coupled with the decrease in grain size (from 90.01 nm to 65.01 nm,), which generally increases the total available scattering area or density of states [8]. These optical findings are consistent with recent research on oxide films grown by PLD. The observed trend of slight absorbance enhancement with increasing laser energy, linked to morphological changes, is in agreement with the results reported by Deng et al. (2021) [27], who found that high PLD energy optimizes the absorption characteristics of metal oxide thin films due to improved structural density [28].

The optical band gap energy (E_g) for the pure GeO_2 thin films deposited at varying laser energies was determined using the Tauc plot method.

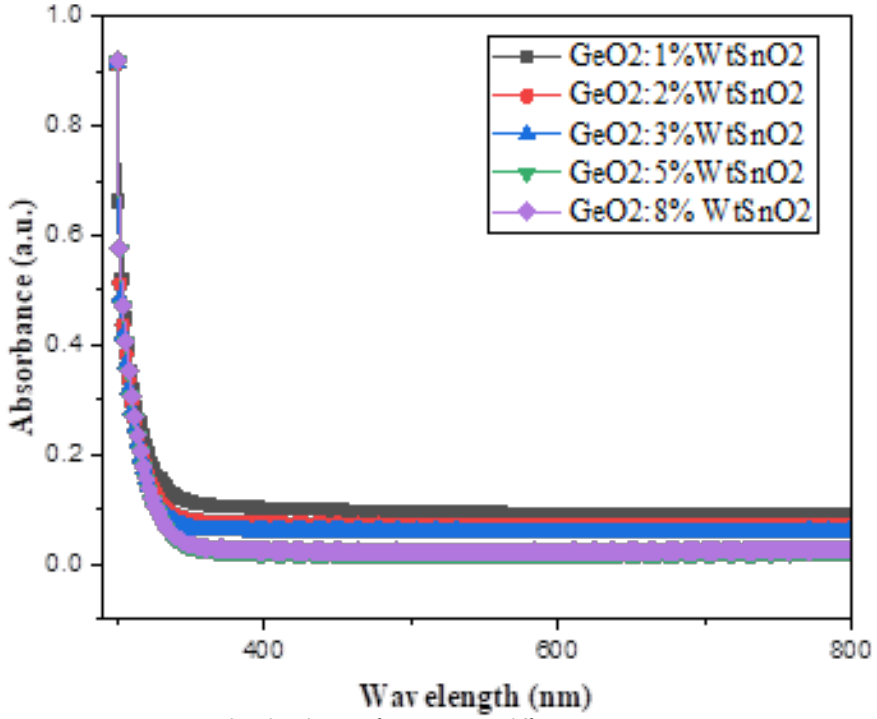

Fig. 13. The Absorbance of GeO_2:SnO_2 at different ratios at 350 mJ.

Table 7. The Absorbance of GeO_2:SnO_2 thin films at laser energy 350 mJ.

Sample	Absorbance (A.U.)
GeO_2:1wt%SnO_2	0.92
GeO_2: 2wt%SnO_2	0.93
GeO_2: 3wt%SnO_2	0.94
GeO_2: 5wt%SnO_2	0.95
GeO_2: 8wt%SnO_2	0.918

The Tauc plots, shown in Fig. 12, display the relationship between photon energy and the absorption coefficient term $(\alpha.hv)^r$, where r=2 for direct transitions. The calculated direct optical band gap energy (E_g) values were found to increase systematically with higher laser deposition energy as shown in Table 6. The E_g value shifts from 3.55 eV at 200 mJ to its maximum of 3.65 eV at 350 mJ. This increase in the optical band gap is primarily attributed to the improvement in the film's structural quality and quantum confinement effects resulting from the high energy PLD process [29, 30]. Higher laser energy promotes a more efficient rearrangement of ablated atoms, leading to films with increased structural density and reduced defects. A decrease in structural defects generally enhances the periodicity of the crystal lattice, widening the band gap [31]. As confirmed by the AFM and SEM results, increasing the laser energy drastically reduces the average particle size (down to 22.24 nm). This size reduction pushes the system into the quantum confinement regime, where the confinement of charge carriers within the smaller nanocrystals leads to a blue shift (increase) in the optical band gap energy [30]. The observed correlation between the enhancement of E_g and the reduction in crystallite size is a well-established phenomenon in semiconductor nanomaterials. This finding is consistent with literature on GeO_2 films [2], and aligns broadly with the general principles of the quantum size effect in nanocrystalline oxides prepared by various methods [31].

The UV-Visible absorption spectra of GeO_2 thin films doped with SnO_2 (1 wt% to 8 wt%) were recorded at a fixed laser energy of 350 mJ. Fig. 13 illustrates the spectra of UV-Vi's absorption spectrum of all doped films showed a fundamental absorption edge, with the maximum absorption occurring consistently around 290nm, characteristic of GeO_2 electronic transitions. A systematic trend was observed in the magnitude of absorption: the absorbance generally increases with increasing SnO_2 doping concentration. The

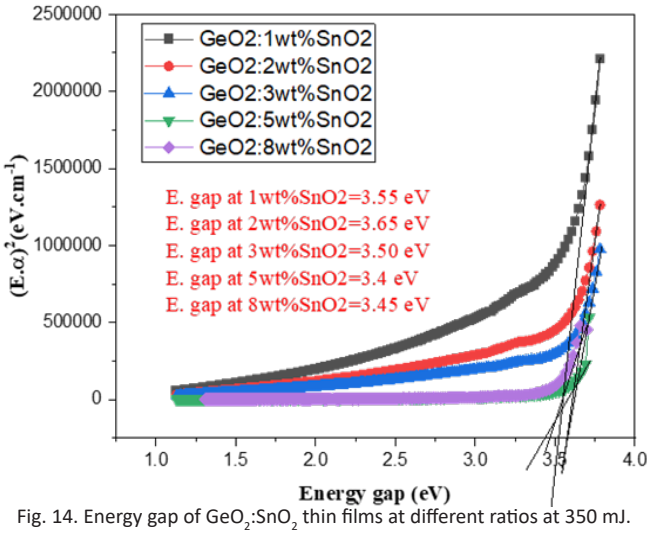

Fig. 14. Energy gap of GeO_2:SnO_2 thin films at different ratios at 350 mJ.

Sample	Direct Band Gap (Eg) (eV)	Trend
GeO_2:1wt%SnO_2	3.55	Increasing
GeO_2: 2wt%SnO_2	3.65	Maximum (Eg Widening)
GeO_2: 3wt%SnO_2	3.50	Decreasing
GeO_2: 5wt%SnO_2	3.40	Decreasing
GeO_2: 8wt%SnO_2	3.45	Stabilizing (Narrowing)

maximum absorbance (A = 0.95) was reached at the 5 wt% concentration, with a slight drop observed at 8 wt% (A = 0.918). This general enhancement in absorbance up to 5 wt% SnO_2 is primarily attributed to the augmentation of the optical path length and changes in film structure induced by the dopant [32]. Sn incorporation can lead to a thicker film [33], increasing the number of absorbing particles. Additionally, structural disorder introduced by the dopant (as suggested by increased AFM roughness, Section 3.3) may introduce localized defect states or enhanced surface scattering, contributing to higher absorbance [34]. The slight drop at 8 wt% may be due to phase segregation or high surface roughness leading to increased light scattering. This correlation between increased dopant concentration and enhanced UV absorption aligns with prior findings in the literature [31, 32].

The direct optical band gap energy (E_g) for SnO_2-doped GeO_2 thin films was determined using the Tauc method, as shown in Fig. 14. The calculated E_g values (Table 8) show a non-monotonic dependence on SnO_2 concentration, indicating a complex influence on the electronic structure. The band gap initially widens from 3.55 eV at 1 wt% to a maximum of 3.65 eV at 2 wt%. It then narrows progressively, reaching a minimum of 3.40 eV at 5 wt%, before slightly increasing to 3.45 eV at 8 wt%. This dual behavior stems from a competition between two dominant effects. At low doping (1wt% and 2 wt%), the initial E_g increase (blue shift) is linked to enhancement of the crystal structure (atomic rearrangement) [35] and, potentially, minor quantum confinement effects. Conversely, at higher doping (3 wt% and above), the band gap begins to narrow due to the formation of secondary energy levels (intermediate levels) within the forbidden gap [36]. These intermediate levels, arising from high dopant concentration and defects, facilitate lower-energy electron transitions, effectively reducing E_g [34]. This non-monotonic dependence is common in doped metal oxides, reflecting the complex interplay between quantum confinement and impurity-induced defect states [36].

CONCLUSION

This study demonstrates that the Pulsed Laser Deposition (PLD) technique successfully synthesized GeO_2 and SnO_2-doped GeO_2 thin films with precisely tunable properties. Increasing the laser energy from 200 to 350 mJ significantly enhanced the crystallinity, increasing the crystallite size to 29.23 nm, and promoted grain refinement that reduced nanoparticle size to 22.24 nm, leading to a widened optical band gap (E.g) due to the quantum confinement effect. In contrast, SnO_2 doping acted as a major structural modifier, inducing a mixed-phase regime (Hexagonal GeO_2 and Tetragonal SnO_2) and increasing the crystallite size up to 58.19 nm. Morphologically, while laser energy led to smaller particles with slight roughness, SnO_2 doping caused significant grain agglomeration (up to 105.34 nm) and a shift toward a three-dimensional island-like growth pattern with increased surface roughness. Optically, SnO_2 doping exhibited a dual effect, initially widening the band gap at low concentrations before causing it to narrow at higher levels (>2 wt%). Ultimately, while high laser energy is essential for maximizing structural quality and band gap width, SnO_2 doping provides a versatile tool for tuning the absorption and electronic states of GeO_2 films for optoelectronic applications.

CONFLICT OF INTEREST

The authors declare that there is no conflict of interests regarding the publication of this manuscript.

REFERENCES

1. Janotti A, Van de Walle CG. Fundamentals of zinc oxide as a semiconductor. Rep Prog Phys. 2009;72(12):126501.
2. Nalam PG, Das D, Tan S, Ramana CV. Controlled Phase Stabilization Enabled Tunable Optical Properties of Nanocrystalline GeO_2 Films. ACS Applied Electronic Materials. 2022;4(6):3115-3124.
3. Golhani DK, Khare A, Krishna BG. Effect of excitation wavelength and silver concentration on the biosynthesized GeO_2 nanocrystals. Inorganic and Nano-Metal Chemistry. 2024;55(8):1003-1017.
4. Gupta AA, Arunachalam S, Cloutier SG, Izquierdo R. Fully Aerosol-Jet Printed, High-Performance Nanoporous ZnO Ultraviolet Photodetectors. ACS Photonics. 2018;5(10):3923-3929.
5. Chen C, Xue M, Liu Y, Zhao L, Yang Y, Hu X, et al. Switchable supermode emission in a doubly-coupled-ring system for multifunctional integrated photonic devices. Opt Lett. 2023;48(14):3705.
6. Gorokhov EB, Volodin VA, Marin DV, Orekhov DA, Cherkov AG, Gutakovskii AK, et al. Effect of quantum confinement on optical properties of Ge nanocrystals in GeO_2 films. Semiconductors. 2005;39(10):1168-1175.
7. Nouri SB, Maieed ZN, Mahmood ASH. The Effect of the Number of Laser Pulses on Some Physical Properties Affecting Gas Sensitivity of CdO Thin Films Prepared by PLD Method. Neuroquantology. 2022;20(3):271-278.
8. Adamik M, Barna PB, Tomov I. Correlation between texture and average grain size in polycrystalline Ag thin films. Thin

Solid Films. 2000;359(1):33-38.
9. Shuaishuai J, Wan X, Cuimin Z, Feihu L, Bo M, Zili Z. Improving the formaldehyde gas sensing performance of the ZnO/SnO_2 nanoparticles by PdO decoration. Journal of Materials Science: Materials in Electronics. 2019;31(1):684-692.
10. Gaser MN, Moghaddam HM, Mutter MM. Pulsed Laser Deposition of GeO_2/Si Thin Films: Tailoring Gas Sensing Performance for NH_3 and NO_2 through Laser Energy Control. Journal of Materials Science: Materials in Electronics. 2025;37(1).
11. Das AK, Misra P, Kukreja LM. Effect of Si doping on electrical and optical properties of ZnO thin films grown by sequential pulsed laser deposition. J Phys D: Appl Phys. 2009;42(16):165405.
12. Scherrer P. Bestimmung der inneren Struktur und der Größe von Kolloidteilchen mittels Röntgenstrahlen. Kolloidchemie Ein Lehrbuch: Springer Berlin Heidelberg; 1912. p. 387-409.
13. Sreeja VG, Hajara P, Reshmi R, Anila EI. Effects of reduced graphene oxide on nonlinear absorption and optical limiting properties of spin coated aluminium doped zinc oxide thin films. Thin Solid Films. 2021;722:138580.
14. Ganesh T, Rajesh S, Xavier FP. Effect of Al dopant concentration on structural, optical and photoconducting properties in nanostructured zinc oxide thin films [Mater. Sci. Semicond. Process. 16 (2) (2013) 295–302]. Mater Sci Semicond Process. 2013;16(6):1718.
15. Influence of Zn doping on structural, electrical and optical properties of SnO_2 thin films. Journal of Xidian University. 2020;14(8).
16. Li B, Rahaman I, Ellis H, Duersch BG, Anderson K, Fu K. Phase Evolution and Substrate-Dependent Nucleation of Quartz GeO_2 Films Grown by Metal-Organic Chemical Vapor Deposition on r- and c-Plane Sapphires. physica status solidi (a). 2025;222(22).
17. Issa MA, Aadim KA. Study the structural and optical properties of Zinc Oxide prepared by pulse laser deposition. Journal of Optics. 2024;55(1):755-760.
18. Editorial Board. Thin Solid Films. 2023;781:140012.
19. Nalam PG, Das D, Shutthanandan V, Ramana CV. α-Quartz Phase Stabilization, Surface Texturing, and Tunable Optical Properties of Nanocrystalline GeO_2 Films Made by Pulsed-Laser Deposition: Implications for Optical and Optoelectronic Applications. ACS Applied Optical Materials. 2023;1(11):1761-1776.
20. Thompson CV. Grain Growth in Thin Films. Annu Rev Mater Sci. 1990;20(1):245-268.
21. Haverkamp JD, Bourham MA, Du S, Narayan J. Plasma plume dynamics in magnetically assisted pulsed laser deposition. J Phys D: Appl Phys. 2008;42(2):025201.
22. Sharma U, Kumar A, Thomas R. Electrical properties of pulsed laser-deposited $Hf_{0.75}Zr_{0.25}O_2$ thin films on platinized silicon substrates. Journal of Materials Science: Materials in Electronics. 2026;37(8).
23. Kaur N, Sharma SK, Kim DY, Sharma H, Singh N. Synthesis of Imine-Bearing ZnO Nanoparticle Thin Films and Characterization of Their Structural, Morphological and Optical Properties. Journal of Nanoscience and Nanotechnology. 2015;15(10):8114-8119.
24. Antoja-Lleonart J, Ocelík V, Zhou S, de Hond K, Koster G, Rijnders G, et al. Growth and Crystallization of SiO_2/GeO_2 Thin Films on Si(100) Substrates. Nanomaterials. 2021;11(7):1654.
25. Kim JH, Lee JB, Kim H, Kim D, Ihm Y, Choo WK. Characteristics of cobalt-doped zinc oxide thin films prepared by pulsed laser deposition. IEEE International Digest of Technical Papers on Magnetics Conference: IEEE. p. GW7.
26. Saravanakumar K, Sakthivel P, Sankaranarayanan RK. Influence of Sn4+ ion on band gap tailoring, optical, structural and dielectric behaviors of ZnO nanoparticles. Spectrochimica Acta Part A: Molecular and Biomolecular Spectroscopy. 2022;267:120487.
27. Deng G, Saito K, Tanaka T, Arita M, Guo Q. Pulsed laser deposition growth of ultra-wide bandgap GeO_2 film and its optical properties. Appl Phys Lett. 2021;119(18).
28. Horiuchi T, Kato Y, Sugino T. Three-layer ionic polymer–metal composite actuator with functionalized carbon nanotubes incorporated into Nafion. Sensors and Actuators A: Physical. 2023;352:114178.
29. Hong Y, Wei Q, Liang X, Lu W. Origin and strain tuning of charge density wave in LaTe3. Physica B: Condensed Matter. 2022;639:413988.
30. Lv H, Xing Y, Wang Y, Li X, Zhang X, Du X. Exploration of accessibility of internal pore surface by using rigid nanoparticles as a probe for constructing the integrated nanocomposites. J Alloys Compd. 2020;815:152641.
31. Optical Characterization of Microstructures and Optoelectronic Devices Based on Wide Band Gap Semiconductors. Wide Bandgap Semiconductors: Springer Nature Singapore; 2025.
32. Rathore MS, Vinod A, Angalakurthi R, Pathak AP, Thatikonda SK, Nelamarri SR. Role of oxygen pressure on the structural and photoluminescence properties of pulsed laser deposited GeO_2 thin films. Physica B: Condensed Matter. 2022;625:413466.
33. Rahaman I, Li B, Ellis HD, Anderson K, Liu F, Scarpulla MA, et al. Phase Competition and Rutile Phase Stabilization of Growing GeO_2 Films by MOCVD. ACS Applied Electronic Materials. 2026;8(5):2015-2023.
34. Ziat Y, Belkhanchi H, Zarhri Z, Laghlimi C. Theoretical Study of the Optical, Structural and Electronic Properties of Germanium Dioxide (GeO_2) Doped with Ti and Nb by the DFT Method with mBJ Correction. NanoRevolution: CRC Press; 2025. p. 195-211.
35. Lee S, Yun E-J. Effects of Bismuth Doping on the Properties of CuO_x Thin Films. Electronic Materials Letters. 2023;19(4):398-404.
36. Possin GE, Adler MS, Baliga BJ. Measurements of band gap narrowing in heavily doped epitaxial emitters and the modeling of heavily doped silicon. 1980 International Electron Devices Meeting: IRE; 1980. p. 270-275.